Agricultural and Forest Meteorology 388 (2026) 111315

Contents lists available at ScienceDirect

Agricultural and Forest Meteorology

journal homepage: www.elsevier.com/locate/agrformet

A characterization of local spatio-temporal variability in daytime occurrence of fog along the Oregon coast using public cameras and airport weather metrics

Sonya Rauschenbach [a,*], John B. Kim [b], Alex W. Dye [e,c], Ian Faloona [d], R. Cotton Rockwood [e], Christopher J. Still [e], Kyaw Tha Paw U [d], Adele L. Igel [d]

[a] Atmospheric Science Graduate Group, University of California, Davis, CA, USA
[b] USDA Forest Service Western Wildland Environmental Threat Assessment Center, Corvallis, OR, USA
[c] Department of the Oregon State Fire Marshal, Analytics and Intelligence Unit, Salem, OR, USA
[d] Department of Land, Air and Water Resources, University of California, Davis, CA, USA
[e] Department of Forest Ecosystems and Society, Oregon State University, Corvallis, OR, USA

ARTICLE INFO

Keywords:
Image analysis
Coastal fog
Ecohydrology
Pacific northwest

ABSTRACT

Fog is a key part of the hydrological cycle in many regions of the world. Coastal fog specifically influences coastal biomes and impacts maritime activities and commerce. Due to complex interactions with landforms, the spatial distributions of coastal fog frequency defy simple characterization. This study is the first to analyze the summertime spatio-temporal heterogeneity of fog along the Oregon coast, a region which depends on coastal fog for shading and as a hydrological input during its warm, dry summers. Direct measures of fog require expensive optical instrumentation that is not broadly deployed. To increase the spatial coverage of in-situ fog records, we used publicly available coastal imagery data sets to detect fog presence at low cost. The coastal imagery consisted of six camera sites located along central and northern Oregon beaches that spanned a 150 km distance. We analyzed the spatio-temporal patterns of this dataset in conjunction with surface weather metrics from the Newport Municipal Airport, which included a visibility sensor for precise fog measurements. We found that the timing of fog occurrence and the overall fog frequency along the coast varied across the locations. Despite this heterogeneity, we found that the average monthly fog frequency at the camera sites had a moderate linear relationship to different metrics of fog and low cloud presence at the airport, suggesting that the airport fog measurements were a reasonable proxy for relative changes in spatially averaged fog frequency. We also found that when there was fog at a camera site, weather conditions at the airport (high relative humidity, low wind speed and lifting condensation level) tended to be supportive of fog formation. However, we found surface weather conditions at the airport were insufficient for real-time fog detection at any particular site along the coast, highlighting the need for more in-situ fog measurements.

1. Introduction

Along the Oregon coast, persistent fog and low clouds are an important source of moisture for dune and forest ecosystems (Dye et al., 2024). During the dry summer season, the terrestrial water cycle depends on the inland incursion of fog and low clouds from the marine layer. Fog and low clouds both lower daytime temperatures and reduce evapotranspiration stress (Williams et al., 2008; Iacobellis and Cayan, 2013). Unlike low clouds, fog can directly supply water to an ecosystem. For example, when vegetation is immersed in fog, water droplets coalesce onto the plant structure and subsequently drip to the soil, providing moisture that can be taken up by plant roots (Carbone et al., 2013; Fischer et al., 2009; Baguskas et al., 2016b). Furthermore, certain plant species are able to absorb water through their leaves, which provide a direct pathway for fog to enhance plant water content (Limm et al., 2009; Baguskas et al., 2016a).

In order to better understand how the variability in fog occurrence impacts the health of these coastal ecosystems, it is important to characterize the spatio-temporal patterns, particularly during the dry summer when fog water serves as a predominant moisture source. A widely used approach to study summertime fog and low clouds along the northern Pacific coast is analysis of geostationary satellite images.

* Corresponding author.
E-mail address: srauschenbach@ucdavis.edu (S. Rauschenbach).

https://doi.org/10.1016/j.agrformet.2026.111315
Received 15 February 2026; Received in revised form 12 May 2026; Accepted 16 June 2026
Available online 24 June 2026

These images offer high temporal resolution but are unable to differentiate between fog, low clouds, or a combination (Clemesha et al., 2016; Dye et al., 2020; Torregrosa et al., 2016; Rastogi et al., 2016). This is a limitation on parsing out how fog distinctly impacts ecosystem functioning compared to other low clouds with bases ranging up to two kilometers from the surface. In situ measurements of fog are available through the Automated Surface Observing System (ASOS) network, a critical source of surface weather metrics that supports aviation. Research using this network to analyze Pacific coast fog has found an overall decreasing trend in fog frequency, which could impact coastal ecosystems that rely on fog (Johnstone and Dawson, 2010; Schwartz et al., 2014). While the ASOS network is a paramount data source, it has only 30 locations along the 1600 km coastline, which leaves much of the Pacific coast understudied. Coastal fog is highly variable in space and time (Bergot and Koracin, 2021): as fog moves inland, the coastal topography and interacting wind patterns create spatial heterogeneity in fog occurrence along the coast (Burk and Thompson, 1996). It is unknown if the ASOS in-situ measurements are representative of the larger area, both due to spatial heterogeneity and distinct properties of airports. Airports are often near urban areas, which have been shown to decrease fog presence (Williams et al., 2015; Izett et al., 2019). Due to the reliance on the ASOS dataset to understand coastal fog, it is important to establish how representative this network is to the surrounding area.

The ASOS network includes sensors that provide measurements of fog because real-time detection of fog is critical for aviation safety. While these sensors are highly accurate, they are costly. In order to address this financial challenge in fog research, digital RGB (red, green and blue) and infrared cameras have been used to detect fog with a binary metric (fog present or not present) over the past decade (Bassiouni et al., 2017; Zhang et al., 2015; Pagani et al., 2018). There is a notable body of research on detecting fog using cameras from the Royal Netherlands Meteorological Institute, Wauben and Roth (2016), Ramlakhan (2015) and Pagani et al. (2018). Webcams have also been used for fog detection in multiple montane cloud forests (Li et al., 2022; Bassiouni et al., 2017; Bendix et al., 2008; Schulz et al., 2014). Additionally, webcams have been used to detect coastal fog (Zhang et al., 2015) as well as the height profile of coastal fog (del Río et al., 2021). However, in these cases, cameras were installed specifically for the research. While there is great benefit to having control over the camera set up, utilizing existing public camera networks can significantly increase the spatial coverage of and access to fog records since there is no incremental instrumentation cost.

In this study, we present a novel approach to detect fog with images from public webcams along the Oregon coast. Our aim was to develop a methodology that robustly detected reduced visibility scenes in order to increase the spatial coverage of fog trends using existing infrastructure. The use of public webcams to get wider coverage of fog occurrence came at the cost of having control over the camera setup and choice of landmarks in the image. This challenge required developing an image-based classification method that is reliable even with non-standardized camera setups (e.g., varying resolution, viewing angles and heights). Each of the camera sites had different background features, and the focus of the cameras was liable to change over time, so the model could not rely on a fixed reference object. An additional challenge was that a few of the sites had ocean-facing cameras without a notable landmass in view. Despite these challenges, we were able to develop an image-based fog classification model with robust performance relative to human-identified fog presence. We applied our image-based fog detection method to characterize the spatio-temporal daytime fog patterns from May to September at six camera sites along the Oregon coast. We analyzed these fog patterns in conjunction with visibility and other fog-relevant surface weather metrics from a nearby coastal ASOS station. This study sought to answer three key questions: (1) Can public web cameras be used to consistently detect coastal fog? (2) What are the spatio-temporal patterns of fog frequency along the coast? (3) To what extent are fog observations and fog-relevant weather metrics at the nearest ASOS station representative of the fog frequency and occurrence at nearby coastal locations?

2. Methods

2.1. Camera sites

We focused our study on the north-central coast of Oregon, USA, a region with little precipitation and frequent fog and low clouds from the marine layer during the summer season. Over 2022 to 2024 we collected daytime images from May to September at five locations along the Oregon coast from www.surfline.com (hereafter 2022–2024 cameras) a commercial website that provides live video for recreational surfing (Table 1) For 2022, the image data was missing during May and June. Images were saved every 30 minutes. These cameras face either ocean or bay, and are mounted above dunes at varying heights and viewing angles (Fig. 1). We also utilized a long-term image database collected by the Coastal Imaging Lab (CIL) at Oregon State University. The camera was located on Yaquina Head, a hill overlooking the coastline (Fig. 1). The images at Yaquina Head (hereafter Yaquina Head camera) were archived every hour from 2000 to 2019.

The camera resolution was not standard between datasets. The camera pixel size for the 2022–2024 dataset was 1280 × 720. For the Yaquina Head camera the resolution changed from 640 × 480 to 1280 × 960 in 2004. In order to have a consistent pixel size for the fog detection model, we cropped the sky and grass from the images at Yaquina Head (Fig. 1) to be either 640 × 360 or 1280 × 720, depending on the native resolution. We then downscaled all higher resolution camera images to be 640 × 360, which matched the cropped, lower resolution Yaquina Head images from 2000–2004. Image processing was done with the scikit-image library in Python (Walt et al., 2014). Because we used RGB digital cameras, that only detect radiation in the visible wavelengths, we only kept photos corresponding to daylight hours with sufficient light. This corresponded to be 7 am to 7 pm PDT for all summer months except September, which we defined to be 8 am to 6 pm PDT.

2.2. Fog detection method at the camera sites

We trained the image classification model on manually labeled images. Out of 85,993 total images, we labeled 10,147 as either foggy [1436], not foggy [9489] or uncertain [41] based on visual inspection. For the 2022–2024 cameras, we labeled a photo as foggy if there was sufficient visibility reduction in the photo to obscure the horizon and furthest parts of the beach, or for Yaquina Head, where the beach was obscure. Photos which were clear or only had small patches of fog that did not fully obscure the horizon were labeled ‘not foggy’. Please refer to the Supplementary Materials for randomly selected example photos which were labeled as ‘foggy’ and ‘not foggy’. The images that were labeled “uncertain” were primarily due to issues with image quality, which was more prevalent in the Yaquina Head camera than the other sites.

We had one labeler, the principal labeler, assigned to labeling all 10,147 images. Due to the subjective nature of visually assessing fog, we assigned an additional five labelers 1000 images in 2024. We used these labels to (1) quantify the uncertainty in image classification and (2) train a separate model based on the consensus label, where at least half of the labelers agreed that the image is foggy. We then compared the results from the consensus model to the core model over the same time period. Note that the principal labeler tended to label an image as foggy when 4/5 of the additional labelers would label an image as foggy (Figure S1). The results of this analysis are in the Supplementary Materials. For the core model, we used the labels from the principal labeler in order to have a higher number of labeled photos that represented all years of the study.

We tested the nine Fog Aware Statistical Features (Table 2) described in Choi et al. (2015) as input features to the classification model. Fog-containing images receive more scattered light and as a result have lower contrast, fainter color and lower levels of luminance (light intensity per unit area) compared to images without fog. The

Table 1
This table shows descriptive information about the six cameras used in this study, including the location of the camera sites, the years the images were collected, the image sampling frequency, the source of the images, the total images used for fog detection, and the estimated height above sea level (H a.s.l) of the latitude and longitude coordinates of the camera site. The H a.s.l is derived from a 30-meter resolution digital elevation model (Farr et al., 2007).

Site name	Lat	Lon	Years	Sampling	Source	N Photos	H a.s.l (m)
Yaquina Head	44.67	−124.06	2000–2019	1 h	CIL	41,161	109
Agate Beach	44.67	−124.06	2022–2024	30 min	Surfline	9099	14
Otter Rock	44.75	−124.06	2022–2024	30 min	Surfline	8519	31
Pacific City	45.21	−123.97	2022–2024	30 min	Surfline	9298	8
Lincoln City	44.96	−124.02	2022–2024	30 min	Surfline	8954	9
Cannon Beach	45.89	−123.96	2022–2024	30 min	Surfline	8962	16

Table 2
This table shows the nine fog-aware image statistics outlined in Choi et al. (2015) and whether they were calculated with grayscale (I_{gray}) or RGB (I_c) pixels.

Feature name	Pixel variable
Variance of MSCN coefficients	I_{gray}
The Variance of the Vertical Product of MSCN Coefficients	I_{gray}
Sharpness	I_{gray}
Coefficient of Variation of Sharpness	I_{gray}
Root Mean Squared Contrast Ratio	I_{gray}
Image Entropy	I_{gray}
Dark Channel Prior	I_c
Color Saturation	I_c
Colorfulness	I_c

Fog Aware Statistical Features provide metrics for these image properties through quantification of image contrast, luminance and pixel variation. See Choi et al. (2015) for details on the equations and their application to images. We dropped features which did not meaningfully increase model performance. See Figure S9 for a comparison of feature importance, which we compared using the Permutation Feature Importance (Breiman, 2001) and the SHapley Additive exPlanations (SHAP) method (Lundberg and Lee, 2017).

We divided each image into three equally-sized horizontal strips and calculated the nine features separately for each strip to provide information richness for different portions of the image. We tested dividing the image into larger numbers of patches, but there was no significant performance gain. We scaled all input features to a normal distribution with a mean zero and standard deviation of one. We trained a Gaussian Process (GP) classification model (Rasmussen and Williams, 2006) on all sites, implemented with the python package scikit-learn (Pedregosa et al., 2011). We assumed a Radial Basis Function as the covariance kernel with a length scale of 1 and a mean of zero. We used 0.5 as the classification cutoff and ran a 10× Monte-Carlo cross validation (Xu and Liang, 2001) with a 70/30 train/test split. We selected a median performing model to classify photos over the entire time period.

We assessed classification performance using three metrics: precision, recall, and the F1 score (Rijsbergen, 1979). These metrics account for both false positives and false negatives differently to assess model performance. A true positive (TP) is an image that has been manually labeled as foggy and classified by the model as foggy; a true negative (TN) is an image that has been labeled as not foggy and classified as not foggy; a false negative (FN) is an image that has been labeled as foggy but classified as not foggy; and a false positive (FP) is an image that has been labeled as not foggy but classified as foggy. We calculated precision, a measure of classification performance accounting for false positives, as

$$Precision = \frac{\sum(TP)}{\sum(TP + FP)} \quad (1)$$

We calculated recall, a measure of classification performance accounting for false negatives as

$$Recall = \frac{\sum(TP)}{\sum(TP + FN)} \quad (2)$$

The F1 score, which is the harmonic mean of precision and recall, is calculated as:

$$F1 = \frac{\sum(TP)}{\sum(TP + \frac{1}{2}(FP + FN))} \quad (3)$$

We optimized the model on the F1 score because it accounts for both false negatives and false positives, which were equally important for our analysis.

2.3. Meteorological data and fog detection at the ASOS station

The nearest coastal ASOS station is located at the Newport Municipal Airport, hereafter referred to by its International Air Transport Association identifier ONP. ONP is located 145 km south of Cannon Beach, the northernmost camera site, and 10 km south of Yaquina Head and Agate Beach, the southernmost camera sites. ONP is 49 m above sea level and is less than 1 km inland from the coastline. Unlike the camera sites, it is sheltered from the coast by ∼1/2 km of forested area (Fig. 1). ONP is equipped with a visibility sensor at 2 m, a ceilometer to measure cloud base height, and sensors for near-surface air temperature, dew point temperature, relative humidity (2 m), and wind speed and direction (10 m). Standard instrument set up for ASOS is described in Bristol (2017).

The World Meteorological Organization (WMO) defines fog as a horizontal surface visibility reduction of less than one kilometer (WMO, 2024). The fog classification algorithm at the camera sites was trained on images where a human labeler visually assessed reduced visibility scenes, without a fixed reference point that would align with the WMO definition. Therefore, we expanded the definitions of fog at ONP to include mist and very low clouds (VLCs) which have been used in prior fog literature (Johnstone and Dawson, 2010; Isaac et al., 2020). The expanded fog definitions allowed for a range of comparisons to comprehensively determine how well ONP related to the camera sites along the coast. Henceforth, we use the phrase 'WMO fog' to specify when we are referring to the visibility sensor detecting less than one kilometer visibility. We defined mist as a visibility sensor measurements of less than five kilometers and relative humidity greater than 95% (Isaac et al., 2020). Prior research on long-term trends in fog frequency in California and Oregon has defined fog as a cloud base of less than 400 m, an ecologically relevant metric of fog that accounts for the surrounding high-elevation region (Johnstone and Dawson, 2010). Similarly, we included an identification of very low clouds (VLCs), where a ceilometer detected a cloud base at less than 100 m. From all fog definitions, we excluded conditions where precipitation is greater than zero.

To address research question 3, we analyzed the distributions of fog-associated weather at ONP when there was fog versus no fog at each camera site. For this analysis, we computed the lifting condensation level (LCL), the altitude at which a rising air parcel is fully saturated, as

$$z_{LCL} = 0.125 \ \frac{\text{km}}{°\text{C}} \times (T - T_{dew}) \quad (4)$$

where z_{LCL} is the LCL in kilometers (km), T and T_{dew} are temperature and dew point temperature respectively in degrees Celsius (°C), and

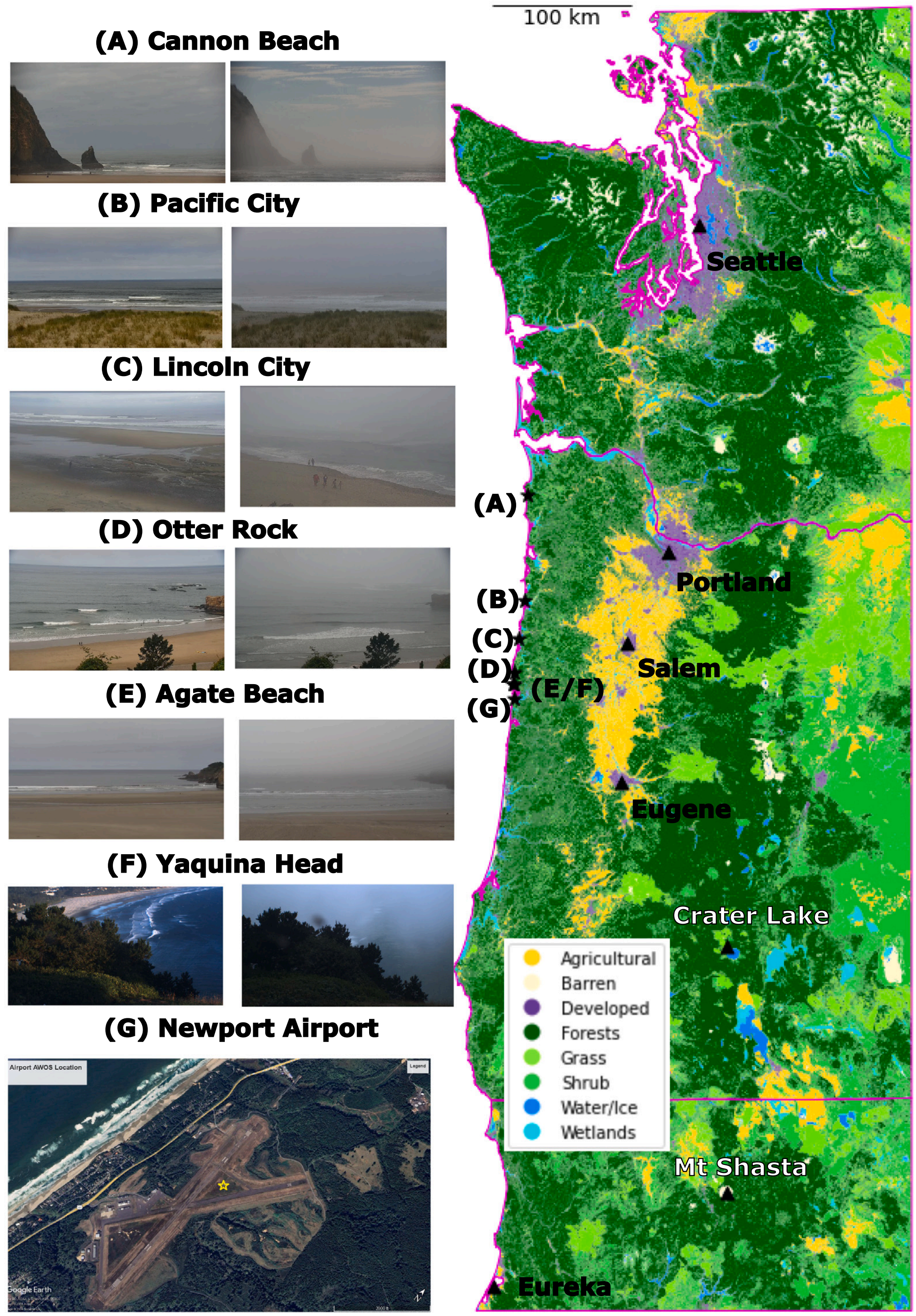

Fig. 1. Locations of cameras and Newport Municipal Airport (coded ONP) on the Oregon coast, with sample images from each camera location with fog and no fog in the image. The location of the ASOS station is marked with a yellow star. Map of land cover from the National Land Cover Database (Earth Resources Observation and Science (EROS) Center, 2025).

0.125 is a constant based on the different rates of change in temperature and dew point temperature under dry adiabatic lifting (Petty, 2008). Other weather metrics were directly reported by the ONP ASOS station.

Additionally, we built a simplified model to gauge the ability of those surface weather metrics at ONP to predict fog occurrence at the camera sites. We fit a logistic regression model with visibility, temperature, LCL, relative humidity, wind speed and wind direction from ONP. This equation is shown in the Supplementary Materials. All weather metrics were standardized to a mean of zero and standard deviation of one. We implemented the model with sklearn using the liblinear algorithm as an optimizer and L2 penalization (Pedregosa et al., 2011).

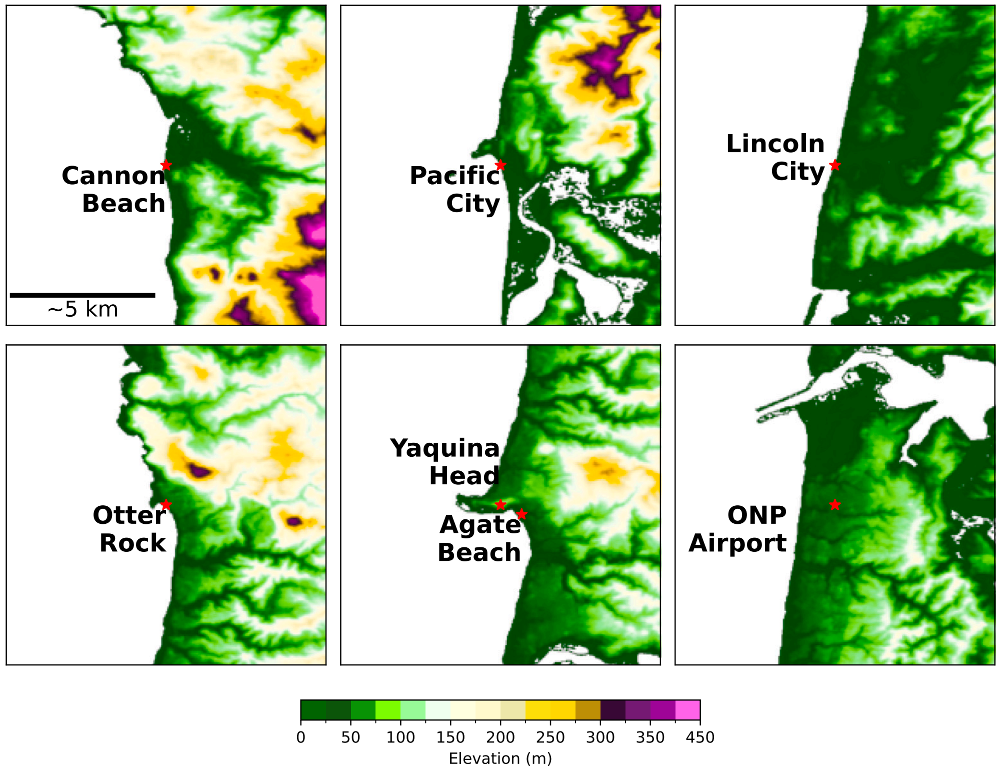

Fig. 2. Topography at camera locations and at Newport Municipal Airport (ONP). Each panel is 10 × 10 km. Elevation estimates are from a 30-meter resolution digital elevation model (Farr et al., 2007). Panels are ordered by site location (north to south), left to right and top to bottom (see Fig. 1 for a regional map). Note the high topographic relief around Cannon Beach, Pacific City, Otter Rock, Yaquina Head and Agate Beach, and that some sites are protected from northerly airflow by a headland. Note also that Newport Municipal Airport is located 1 km from the coastline.

Each site's model was trained individually. To address class imbalance, we included an even number of fog and no fog observations in the training set. We used a 70/30 train test split, repeated with 100× cross validations.

2.4. Spatio-temporal heterogeneity

We analyzed the spatio-temporal heterogeneity of instantaneous fog occurrence, sampled in hourly or half-hourly periods depending on the site, as well as the fog frequency over various timescales. We analyzed fog frequency for daily, weekly and monthly time periods as well as for the diurnal and seasonal cycles to compare spatial patterns in fog frequency over larger time averaging windows. We used a weekly frequency for the seasonal cycle so that there would be enough observations per site for robust statistical analysis. When calculating fog, mist and VLC occurrence and frequency at ONP we only used daytime hours. We were also able to compare the annual summertime fog frequency for the Yaquina Head camera and ONP over the summer months of May to September.

To address Q2, we compared the pairwise correlation between sites for the timescales described above. We used the phi-coefficient, a measure of how two binary variables associate with one another, as the correlation coefficient for instantaneous fog co-occurrence. We used Kendall's tau, a non-parametric rank-based test which is robust for small sample sizes, as the correlation coefficient for fog frequency at all timescales, and a linear regression to analyze how the strength of the correlation related to the distance between sites.

To further address Q3, we fit linear regression models to determine how ONP fog, mist and VLC frequency relates to the fog frequency at the camera sites. We compared the fit between these metrics at ONP and the spatially averaged fog frequency of three sets of camera sites: all 2022–2024 camera sites, the sites closest to the airport (Agate Beach, Otter Rock), which were less than 20 km away, and the sites furthest from the airport (Pacific City, Lincoln City and Cannon Beach), which range 50 to 145 km away. The Yaquina Head camera was the only site with a long time series of fog occurrence. We fit the linear relationship between the fog frequency at ONP and Yaquina Head for the annual daytime summertime fog frequency as well as the percent of summer foggy days from 2001–2019 at Yaquina Head and 2001–2024 for ONP.

Table 3
Fog classification model performance metrics by camera site. Precision, recall and F1 are performance metrics defined in Section 2.2. Numbers of images manually labeled and used in the assessment are given in the last column. The scores reported are the average across all ten cross validations and the ± values are standard deviations.

Site	Precision	Recall	F1	Labeled
Cannon Beach	0.96 ± 0.008	0.78 ± 0.02	0.86 ± 0.01	1597
Pacific City	0.95 ± 0.01	0.91 ± 0.01	0.93 ± 0.005	1662
Lincoln City	0.86 ± 0.008	0.82 ± 0.01	0.84 ± 0.005	1630
Otter Rock	0.82 ± 0.02	0.87 ± 0.01	0.84 ± 0.01	1502
Agate Beach	0.85 ± 0.006	0.84 ± 0.009	0.85 ± 0.006	2025
Yaquina Head	0.95 ± 0.007	0.94 ± 0.007	0.95 ± 0.003	2054

3. Results

3.1. Fog classification model performance

Overall, the GP classification model had an average F1 score of 0.87 ± 0.015, with a precision of 0.90 ± 0.018 and a recall of 0.85 ± 0.023. Model performance by site ranged from 0.84–0.94 (Table 3). The model performance was comparable to other image-based fog classification models that used Fog Aware Image Statistics as input features (Bassiouni et al., 2017; Pagani et al., 2018; Li et al., 2022).

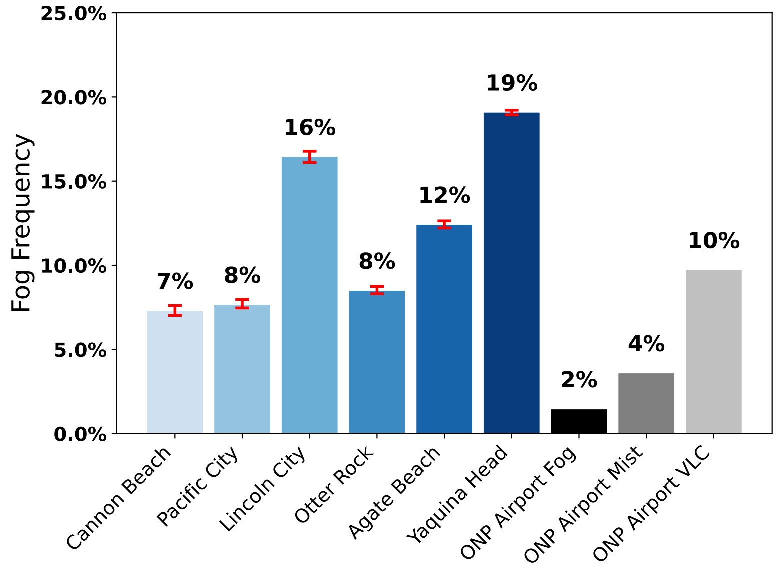

Fig. 3. Fog frequency by site at ONP and classified with the Gaussian Process model. Camera sites are shown in blue, ordered from north to south. The red line shows the minimum and maximum fog percent across all ten cross validations. Fog frequency at ONP is shown in black and gray for the different metrics used. All fog frequencies are for the summer months of May to September during daytime hours (7 am–7 pm, May–Aug; and 8 am–6 pm, Sep). Fog is defined as a horizontal surface visibility reduction of less than one kilometer (WMO, 2024). Mist is less than 5 km visibility and relative humidity greater than 95% (Isaac et al., 2020). Very low clouds (VLC) is the presence of a cloud base less than 100 m (Johnstone and Dawson, 2010).

Additionally, the performance was substantially higher than the previous fog classification model with coastal images (Zhang et al., 2015). Our classification model consistently under-predicted fog relative to labeled data, whereas other models have a less consistent bias across sites (Bassiouni et al., 2017; Li et al., 2022). The Fog Aware Statistical Features generalized well across different image compositions. We did not detect a relationship between model performance and image background structure. For example, the backgrounds of Pacific City and Agate Beach had comparable ratios of shore to ocean in their field of view, yet Agate Beach performance was lower than the overall average and Pacific City was higher. The precision of the classification model was typically higher than the recall, indicating that there were fewer false positives than false negatives. Therefore, the classification model is a conservative estimate of fog occurrence compared to the labeled fog occurrence.

We also compared the model performance by year for the 2022–2024 cameras. The best-performing year was 2022 (F1 score of 0.88 ± 0.011), followed by 2023 (F1 score of 0.82 ± 0.019) and 2024 (F1 score of 0.75 ± 0.022). To determine if the classifications from the lowest-performing year, 2024 lead to meaningfully different results, we compared all analyses in the paper for the year of 2024 from the overall model to the consensus labeled model, which had model performance on par with 2022 and 2023 (F1 score of 0.88, with a precision of 0.93 and a recall of 0.83). We found no meaningful difference for the qualitative conclusions drawn in this study aside from the slightly lower fog frequency determined by the principal labeler (Figures S2–S8).

3.2. Spatiotemporal variability of fog frequency

3.2.1. Overall fog frequency

Fog frequency varied significantly across sites (Fig. 3). At the airport, WMO fog occurred during 2% of daylight hours, whereas VLCs occurred more frequently. The fog frequency at Yaquina Head from 2001–2019 was higher than the other locations (19%). This difference could be because the camera is located about 90 m higher than any other camera and therefore may be detecting VLCs that do not constitute fog closer to sea level (Fig. 2). Fog frequency at the 2022–2024 camera sites varied and was highest at Lincoln City (16%), and lowest at Cannon Beach (7%). The variation in frequency for the 2022–2024 camera sites is not clearly explained by height a.s.l, given that Otter Rock, which is located at higher elevation, shows similar fog frequency to Pacific City and Cannon Beach. The Lincoln City camera is located on a low elevation point, and yet has the highest fog frequency. The surrounding topographic features at the sites may be relevant. The other four 2022–2024 camera sites have more complex surrounding topography than Lincoln City. The lee-side of headlands often have less fog, since headlands can act as a shelter to the marine layer from the predominantly northern winds (Torregrosa et al., 2016). Agate Beach, Cannon Beach, Pacific City and Otter Rock are all sheltered from the prevailing northward winds by a headland (see Fig. 2). The Lincoln City site is unprotected by any headlands to the north or south of the camera site, which may explain why Lincoln City has such high fog frequency. However, more in-situ fog measurements would be necessary to confirm this.

A worldwide study of fog climatology based on ship observations found an average of 6%–11% fog frequency along the Oregon coast in June, July and August from 1950 to 2007 (Dorman et al., 2020). Three out of six of our camera sites show a fog frequency that falls within this range. Ship observations are based on a subjective assessment of fog from a trained observer using landmarks and the horizon, and so the method of characterizing fog has parallels to the labeling methodology in this study (Environment Canada, 2017). However, a direct comparison between the ship observations and the camera observations is difficult, since the ship observations occur during both day and night. The airport has 24 h fog observations, and the ratio of overall WMO fog frequency (2.8%) to daytime WMO fog frequency (2.0%) is 1.4. If we assume this ratio of overall fog frequency to daytime fog frequency for the camera sites, one third of the fog frequency at the camera sites fall within the range described by Dorman et al. (2020) for the Oregon coast.

There are three possible reasons for the substantially lower WMO fog frequency at the airport. (1) WMO fog at the airport was defined with an objective standard of less than one kilometer visibility, whereas the camera dataset was trained on photos which had fog sufficient to obstruct visibility as identified by a human observer. (2) The airport weather station is located ~1 km inland and with vegetated terrain between it and the coastline, whereas the cameras have a clear, unobstructed view of the coast. (3) ONP has distinct surface characteristics

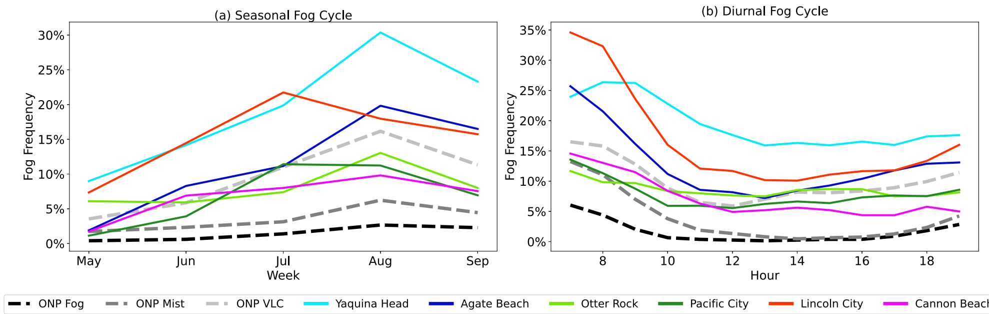

Fig. 4. Seasonal (a) and diurnal (b) cycles of fog frequency at six camera sites and Newport Municipal Airport (ONP). Only daytime images were used from the six camera sites (7 am–7 pm, May–Aug; and 8 am–6 pm, Sep). Fog is defined as a horizontal surface visibility reduction of less than one kilometer (WMO, 2024). Mist is less than 5 km visibility and relative humidity greater than 95% (Isaac et al., 2020). Very low clouds (VLC) is the presence of a cloud base less than 100 m (Johnstone and Dawson, 2010).

that impact wind flow (flat terrain containing two runways, hangars and parking lots) and temperature (albedo and heat capacity of built surfaces and buildings), particularly during daytime when the surface heats up faster than the near-shore ocean. The diurnal mixing can result in a lifted cloud base over land while there is still fog over the ocean. The relative importance of these factors are unknown.

3.2.2. Diurnal and seasonal fog frequency

Seasonal and diurnal fog cycles at all sites exhibited seasonal peaks in mid-to-late summer and in the morning hours (Fig. 4). The majority of sites peaked in August, except for two sites in the middle of the north-to-south transect, Lincoln City and Pacific City, which peaked in July. The seasonal cycles of VLCs at ONP and the nearby Yaquina Head and Agate Beach sites followed similar seasonal patterns. Prior research on the seasonality of fog and low cloud cover for the Northern Hemisphere Pacific coast has found that the seasonal peak depends on the latitude, starting in June for southern California and ending in July for Oregon and Washington (Clemesha et al., 2016). Dye et al. (2020) found that on average, fog and low cloud cover along the PNW coast peaked in July, though cloud coverage remained high through September. Given that the majority of our camera sites show that fog occurrence peaked in August, there may be different seasonal trends for fog versus other low-level clouds. However, there was heterogeneity across the five in-situ sites, and they represent a considerably smaller sample of the coast than satellite imagery can provide.

All sites and fog metrics showed a diurnal cycle observed in prior fog research (Torregrosa et al., 2014; Lundquist and Bourcy, 2000; Filonczuk et al., 1995), with peak fog occurrence in the morning hours, then a decrease throughout the day. Lincoln City, Agate Beach and ONP fog metrics had notable upticks in fog frequency during the evening hours. These results are typical for Pacific coast fog (Torregrosa et al., 2014; O'Brien et al., 2013; Filonczuk et al., 1995; Lundquist and Bourcy, 2000).

3.2.3. Asynchrony of fog occurrence

Fog occurrence was spatially variable between the 2022–2024 camera sites and ONP (Fig. 5). Most pairwise correlations in instantaneous fog occurrence were less than 0.4. WMO fog had a very low correlation with the camera sites, and VLCs had comparable correlations to the camera sites as the camera sites did to one another. The highest correlation was between Agate Beach and Otter Rock, which were located only 8 km away from each other. Fog was most likely to occur at only one site at a time, and 63% of all fog instances were only at one or two sites. It was very rare that fog occurred at 5 or all sites simultaneously (Fig. 5). Note that for this analysis, we consider fog co-occurring between ONP and any number of camera sites if there was fog, mist, or VLCs present to give the most expansive opportunity for co-occurrence to happen. Even with this most expansive definition of fog at ONP (fog, mist, or VLCs), co-occurrence between many sites within the same half hour is still rare. It was more common for fog to occur at multiple sites on the same day, even if not at the same time of day: over 50% of fog days were days on which fog occurred at three or more sites, and it was slightly more likely that fog occurred at six sites than at two sites on the same day.

3.2.4. Correlations of fog frequency across timescales

At shorter timescales, the strength of the correlation between camera sites was inversely proportional to the distance between sites (Fig. 6). The negative slope of a linear fit between pairwise site distance and pairwise site correlation was statistically significant for instantaneous fog co-occurrence, quantified by the phi correlation coefficient, and for daily fog frequency, quantified by the Kendall's Tau correlation. This negative relationship is true even when ONP is included, indicating that the presence of fog, mist and/or VLCs on the daily or instantaneous timescales follows a similar pattern to the pairwise relationship between camera sites. At the monthly, diurnal and seasonal timescales, there is no statistically significant relationship between two sites' distance and their seasonal fog frequency. These findings demonstrated that at shorter timescales, fog patterns were more closely related at nearby sites, but after the daily timescale, distance was not a key factor.

3.3. Relation of airport surface weather metrics to fog frequency along the coast

3.3.1. Airport fog frequency as predictor of the average coastal fog frequency

WMO fog, mist and VLC frequency at ONP had varying linear relationships to the spatial average of fog frequency along the coast (Fig. 7). For WMO fog, there was no evidence that the airport was more predictive of fog at closer coastal locations, given comparable R^2 value for closer camera locations and similar best-fit slopes. However, the overall relationship was moderate (R^2 of 0.50 and Kendall's Tau of 0.49). One should also note that this analysis has a small sample size (13 observations) and that the strength of this linear relationship hinges on the inclusion of the two lowest observed fog frequencies. For this reason, we also showed the Kendall's Tau coefficient, which is robust for small datasets because it does not assume a normal distribution. The Kendall's Tau correlation showed a statistically significant positive relationship. Mist at ONP related more strongly to the overall average and to the closer sites, and VLCs showed the strongest relationship to the spatially-averaged fog frequency at the camera sites. The strength of this relationship differed for the sites which were nearby versus those that were further away, however overall the amount of variance in the spatially averaged fog frequency at the camera sites which explained by VLC presence at the airport was high ($R^2 = 0.75$ for site less than 20 km away and $R^2 = 0.59$ for sites further). These results demonstrated that WMO fog, mist and, in particular, VLCs at the airport were a good proxy for the average coastal fog frequency, indicating that there was still information to be gained from monthly average fog trends at the airport for a 150 km swath of coast.

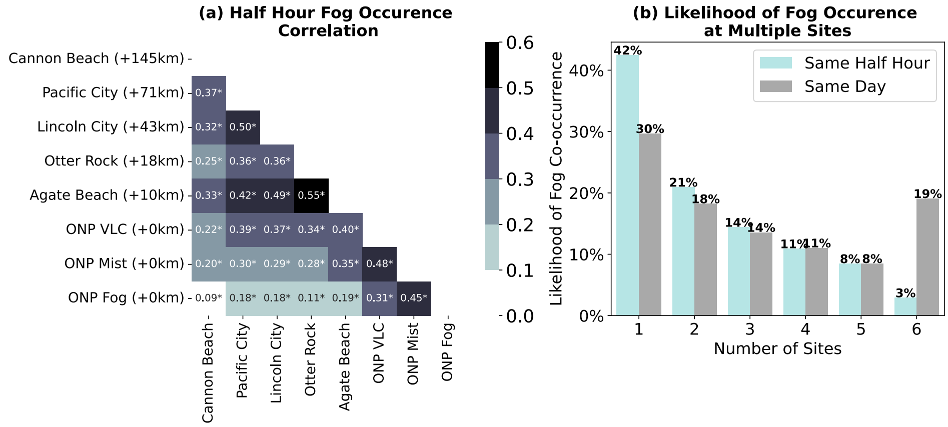

Fig. 5. Pairwise correlation (ϕ) of instantaneous fog occurrence between all sites (a). Stars denote statistical significance at the 0.95 confidence level. Distances from camera locations from Newport Municipal Airport (ONP) are given in the Y-axis. Likelihood that fog will occur at a given number of sites at the same sampled 30 min. interval or on the same day (b). Fog is defined as a horizontal surface visibility reduction of less than one kilometer (WMO, 2024). Mist is less than 5 km visibility and relative humidity greater than 95% (Isaac et al., 2020). Very low clouds (VLC) is the presence of a cloud base less than 100 m (Johnstone and Dawson, 2010).

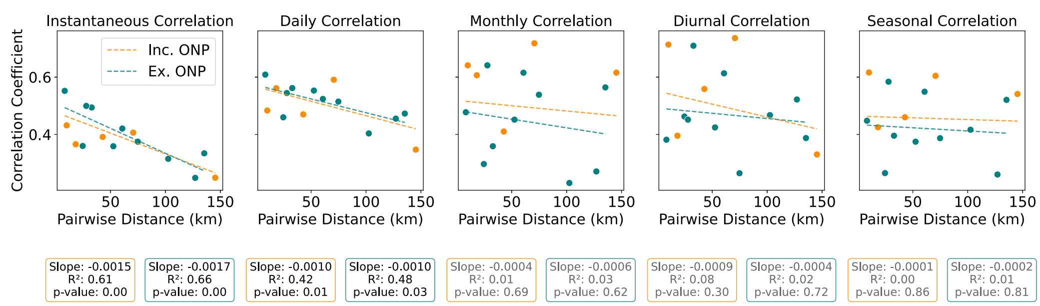

Fig. 6. Correlation in fog frequency across sites as a function of the Euclidean distance between pairs at multiple time scales. Correlation between the camera sites are shown in teal, correlations between each camera site and Newport Municipal Airport (ONP) are shown in orange. The dashed lines show the linear trend of an ordinary least square regression, both including and excluding correlations between the camera sites and ONP. The slope, R^2 and p-value of this linear trend are below each plot, shown in black when statistically significant and gray when not. The orange line and box show the regression result using all camera sites and ONP, the teal line and box show the results for only the camera sites. Fog is defined as a horizontal surface visibility reduction of less than one kilometer (WMO, 2024). Mist is less than 5 km visibility and relative humidity greater than 95% (Isaac et al., 2020). Very low clouds (VLC) is the presence of a cloud base less than 100 m (Johnstone and Dawson, 2010).

3.3.2. *Long-term fog frequency at Newport Municipal Airport and Yaquina Head*

The Yaquina Head camera site and ONP were the only locations with time series long enough to analyze annual trends in fog frequency. There was no statistically significant trend in fog frequency or the percent of foggy days for the time series at Yaquina Head from 2001–2019 (Fig. 8). There was a statistically significant negative trend in fog frequency at ONP (a 0.05% decline annually), but no significant trend in the percent of foggy days. Neither was there any statistically significant linear trend in mist or VLC frequency over the analyzed time period.

3.3.3. *Distribution of fog-associated surface weather metrics*

There were large, statistically significant differences in all fog-relevant weather metrics at ONP when fog was detected at any camera site similar to the differences when WMO fog, mist or VLCs were detected at the airport (Fig. 9). When fog was present at a camera site, ONP has distinctly high relative humidity, low cloud bases and LCL height, and typically, but not always, reduced visibility and weaker winds that are more likely southwesterly than when fog was not present. Lower wind speeds and a proclivity for wind from the southwest has been associated with fog weather in prior research of Oregon fog (Lundquist and Bourcy, 2000). Southwest winds in particular have been associated with the phenomena of coastally trapped wind reversals, which are known to bring foggy conditions to California and Oregon (Nuss et al., 2000). When fog was not present at a camera site, the visibility was frequently at its maximum value of 16 km and the LCL heights are substantially larger. These results indicate that even though fog occurrence was much lower at ONP as compared to the camera sites, weather conditions are often primed for fog. The results are also remarkably similar across camera sites. The higher likelihood of fog-associated weather reported at the airport when fog was detected at any camera site suggests that environmental conditions for fog (high moisture and low wind) along the coast were similar for sites close and far. This suggests some degree of homogeneity in fog-associated weather, even if the when-and-where of fog occurrence is highly variable. The clear evidence of fog weather at the airport when fog was detected at the camera sites also lends additional support to classification model performance.

3.3.4. *Predicting fog on the coast with airport weather metrics*

The logistic regression model of fog occurrence performed moderately well only at three sites – at Yaquina Head, Agate Beach and Lincoln City – with median F1 scores ranging between 0.58 and 0.41 (Fig. 10). The model performed poorly at the other three sites, with median F1 scores near or below 0.25. The average precision score of the model across all sites was ~30%, whereas the recall score was ~75%, indicating that the model over-predicts fog more often than it under-predicts fog. Relative humidity and LCL were the strongest predictors with higher magnitude coefficients. The high F1 scores for Yaquina

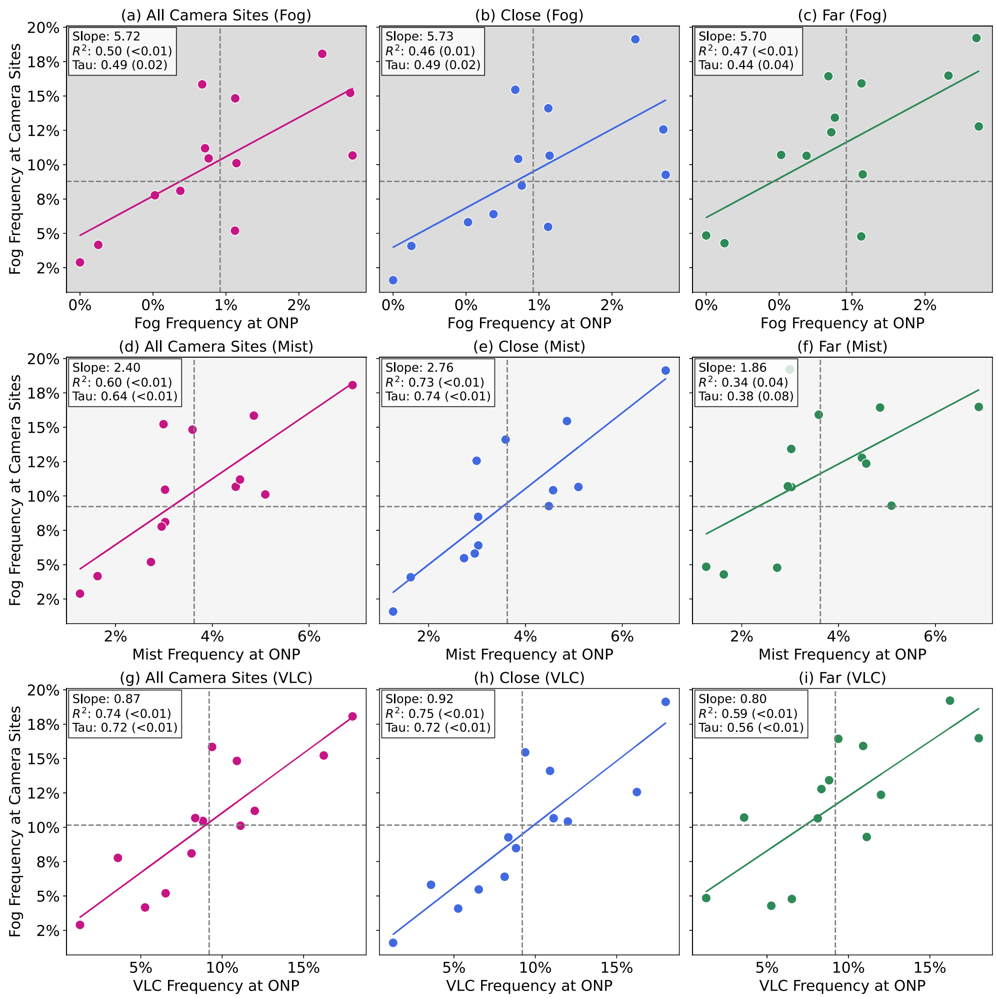

Fig. 7. Correlation of fog frequency at Newport Municipal Airport (ONP) to monthly fog frequency at camera sites. Camera sites close to the airport (Agate Beach, Otter Rock) are plotted separate (b) from those farther away (c) (Lincoln City, Pacific City, Cannon Beach). ONP is south of all camera sites and around one km inland. Trend lines were fitted with ordinary least squares regression. Dotted lines show the average fog frequency along the coast and at the airport for the whole time period. Fog is defined as a horizontal surface visibility reduction of less than one kilometer (WMO, 2024). Mist is less than 5 km visibility and relative humidity greater than 95% (Isaac et al., 2020). Very low clouds (VLC) is the presence of a cloud base less than 100 m (Johnstone and Dawson, 2010).

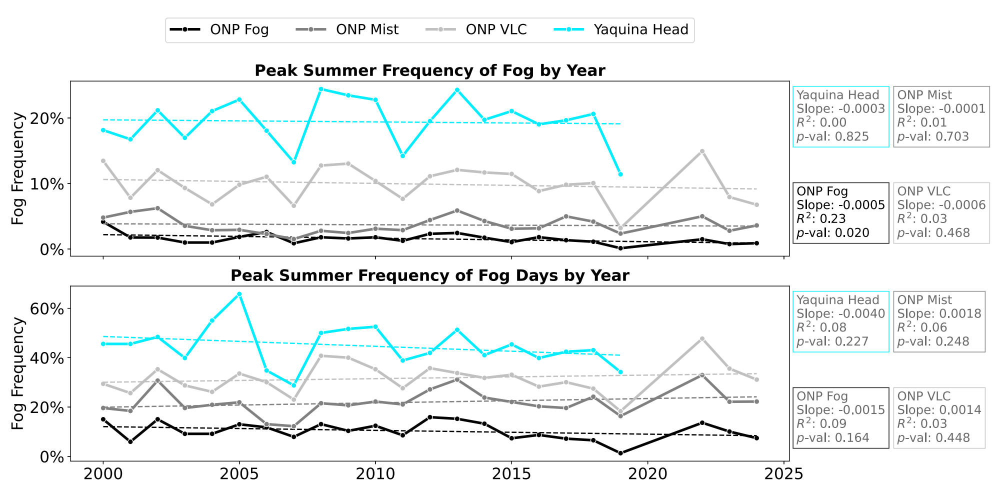

Fig. 8. Long-term trends in summertime fog frequency at Newport Municipal Airport (ONP) and Yaquina Head, 8 km north of ONP (a) and in the percent of foggy days (b). Dashed lines are fitted to data using a linear regression. Linear fit of fog frequency (c) and percent of foggy days (d) between ONP and Yaquina Head is also shown. Fog is defined as a horizontal surface visibility reduction of less than one kilometer (WMO, 2024). Mist is less than 5 km visibility and relative humidity greater than 95% (Isaac et al., 2020). Very low clouds (VLC) is the presence of a cloud base less than 100 m (Johnstone and Dawson, 2010).

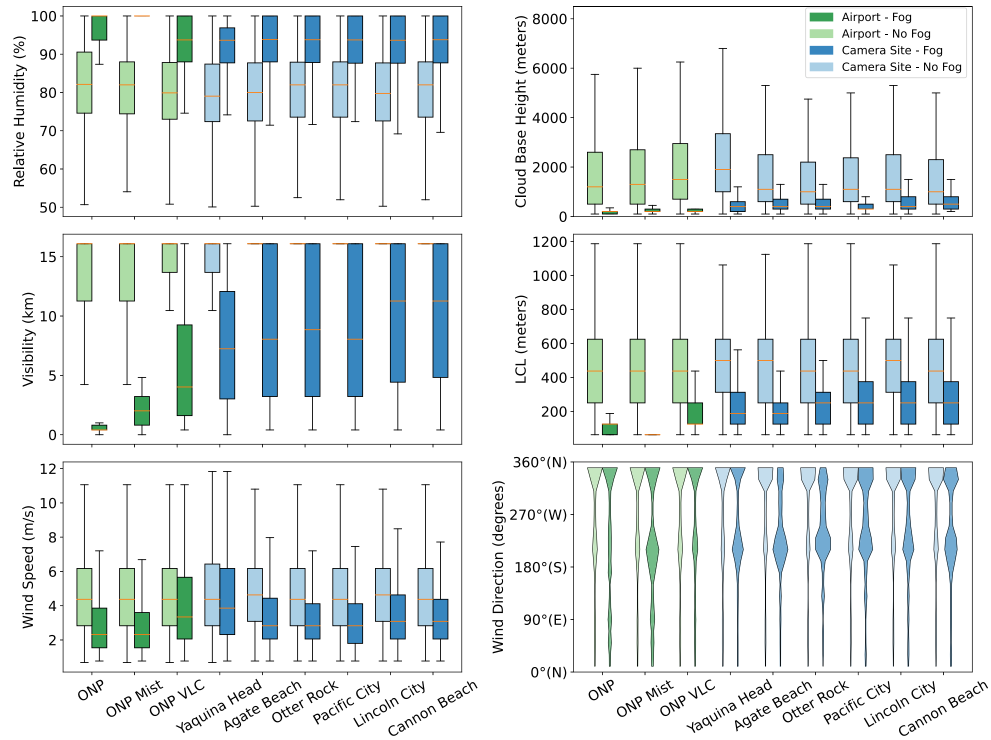

Fig. 9. Boxplots of weather observations at Newport Municipal Airport (ONP) when fog is detected and not detected at any of the camera sites and when WMO fog, mist and VLCs are present at ONP. Fog is defined as a horizontal surface visibility reduction of less than one kilometer (WMO, 2024). Mist is less than 5 km visibility and relative humidity greater than 95% (Isaac et al., 2020). Very low clouds (VLC) is the presence of a cloud base less than 100 m (Johnstone and Dawson, 2010). Boxes represent the 25th and 75th percentiles and the median line is in orange. Whiskers show the 5th and 95th percentiles. Wind direction is shown as a mirrored histogram in order to better visualize wind direction tendencies. Sites are ordered left to right by increasing distance to the airport (south to north). All distributions are statistically significantly different for fog vs. no fog instances, based on the one-sided Kolmogorov–Smirnov test.

Head and Agate Beach may partly reflect its proximity to the airport (they are co-located 10 km from the airport). There also seemed to be a relationship between higher fog frequency and higher F1 scores, since Yaquina Head, Agate Beach and Lincoln City have the top three fog frequencies. These results highlight challenges in fog prediction at coastal sites with basic surface weather metrics at a second location, particularly when fog is infrequent, since fog weather is much more prevalent than fog formation (Bergot and Koracin, 2021).

4. Discussion

Public cameras have become ubiquitous in recent years, offering an untapped resource for analyzing the spatial patterns of fog. This study demonstrated that cameras can be used for analyzing spatio-temporal fog patterns, although many challenges remain. Identifying fog presence without visibility sensors brings subjectivity into the analysis. Fog, mist and haze exist on a continuum, and it can be difficult for the human eye to differentiate them, even with fixed reference points at a known distance (Kim, 2018). Despite these challenges, datasets that utilize human-determined fog presence are critical to understanding spatio-temporal patterns in coastal and marine fog. For example, a worldwide fog climatology used fog identification from the International Comprehensive Ocean-atmosphere Data Set (Dorman et al., 2020). In this dataset, the fog observations were noted by a trained ship crew member, who recorded whether fog was present either by using a landmark at a known distance, or by their subjective judgment of the horizon when no landmark is available (Dorman et al., 2020; Environment Canada, 2017). In our study, to quantify the uncertainty of an individual labeler to the fog classification model, we compared the implied fog frequency of the principal labeler to that of five additional labelers (Figure S1 and accompanying supplementary text). In our analysis, we found that while the principal

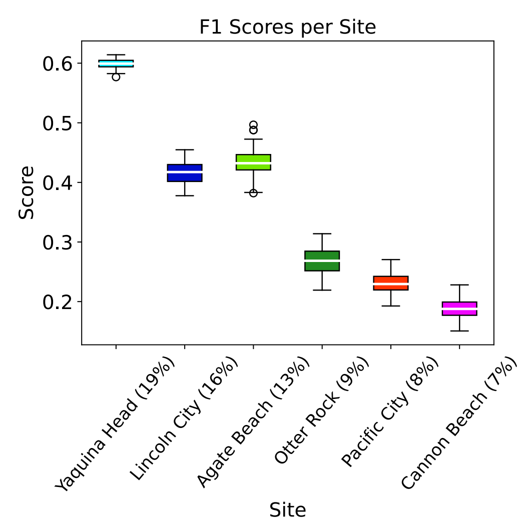

Fig. 10. Performance of a simplified fog prediction model. Logistic regression was applied at the individual camera sites, with weather data from Newport Municipal Airport as independent variables and fog occurrence as the dependent variable. Model accuracy scores (F1) are averaged over 100 replicates at each site. Boxes represent the two inner quartiles and the whiskers represent 5th and 95th percentiles. Open circles present outliers. Sites are ordered by overall observed fog frequency. See Methods for additional details of the prediction model.

labeler designated slightly fewer images as foggy, this difference did not impact the conclusions of the spatiotemporal analysis (Supplementary Materials). However, the absolute value of fog occurrence at the sites has uncertainty arising from visual classification of fog images by humans without the use of a co-located visibility sensor. Finally, the use of public cameras has major limitations. Camera elevation, viewing angles, scene compositions, lighting conditions, hardware, firmware and image storage protocols may be irregular, difficult to document, and may impact fog detection.

To make image-based fog detection more objective, an experiment with co-located visibility sensors and cameras at multiple locations would be critical to determining the direct relationship between optical properties of a forward scatter visibility sensor and RGB cameras. The Fog Aware Statistical Features used in our model are continuous variables designed to isolate the fog signal in the image, remove the fog from the photos and restore the background information (Choi et al., 2015). With these input features, there is potential to establish a relationship between these fog-aware image statistics and visibility or optical depth if visibility sensors were co-located with cameras. Even with a co-located visibility sensor, there are fundamental differences between these sensors and cameras. Forward scatter visibility sensors sample a small volume of air in the path of the sensor and detect scattering in a specific infrared channel, whereas RGB cameras have a wider field of view and detect emitted light in three wide bands in the visible spectra. Another key difference between image-based fog detection and visibility sensors is that the former requires more upfront work to set up the fog detection, including image labeling and model tuning. Applying this study's model to other locations would entail additional labeling. Prior studies have used a similar input features calculations on a wide variety of image backgrounds (Bassiouni et al., 2017; Pagani et al., 2018; Li et al., 2022), but further experimentation and labeling would be required to determine if an out-of-the-box fog classification model could be generalized to other locations. However, after the initial work to train the model, our success using an existing camera infrastructure to detect and analyze fog shows how this methodology can be applied to extant camera networks to monitor, for example, road or port traffic or agricultural fields for either real-time fog detection or fog spatiotemporal analyses, albeit with some uncertainty.

5. Conclusions

Climate change has the potential to modulate the frequency of coastal fog and its inland flow in complex ways. One of the richest datasets to study coastal fog comes from the ASOS weather stations located at airports. However, there has been little research that statistically relates fog occurrence at airport sites to that of the surrounding area. Additionally, coastal fog is highly variable in time and space, yet there have only been a few studies comparing trends in fog frequency across point locations over short distances of roughly 100 to 200 km (Tardif and Rasmussen, 2007). Our study is the one of the few that used ground-based spatio-temporal measurements of fog along the Oregon coast, as opposed to satellite-derived fog and low cloud cover. Our study achieved this using six RGB cameras, five of which were publicly available webcams, and we have demonstrated that this methodology can be used to gain deeper insights into spatial patterns of daytime fog occurrence. We were able to relate our machine learning classified dataset of fog occurrence to fog metrics from a nearby ASOS station. From this analysis, we draw several conclusions:

1. Coastal public web cameras can be used to qualitatively detect fog. When the images are labeled and trained with a consistent method, the resulting fog time series can be used to comparatively assess spatio-temporal patterns.

2. Most frequently, fog was detected at only one site at a time, which demonstrates the patchiness of fog occurrence along the coast. There was more spatial consistency in fog occurring at multiple sites on the same day. It was even slightly more likely for fog to occur at all six locations than at only two locations on a given day.

3. At the daily and sub-daily timescales, the correlation in fog frequency between two sites is strongly related to the distance between them. However, sites closer together had no stronger a correlation between their monthly fog frequency, nor their diurnal and seasonal cycles, than sites further apart.

4. Monthly fog patterns recorded by the ASOS weather station at the Newport Municipal Airport (ONP) are a good proxy for the average monthly fog frequency of the surrounding coastal area. In particular, VLCs correlate strongly to the spatially averaged fog frequency detected at the camera sites ($R^2 = 0.74$).

5. Whenever there is fog at a given coastal location, the ASOS weather station at ONP shows the conditions for fog (high relative humidity, low wind speed, low cloud base and LCL). While this analysis only compares two point locations—the airport and the camera site—it provides some evidence that there is homogeneity in the weather systems supporting fog formation in the distance spanning these sites. However, these statistically significant differences in surface weather metrics did not translate into the predictability of fog occurrence at the camera sites (Fig. 10). Our highly simplified model demonstrated that there are limitations in using basic surface weather instrumentation for fog prediction, because fog-associated weather metrics like high relative humidity and low wind speed occur more frequently than fog formation itself. As such, the logistic regression categorically over-predicted fog occurrence. Such a result points to the value of utilizing camera networks to qualitatively detect fog in real time.

A study utilizing more cameras or other in-situ measurements, with a longer time period and co-located weather metrics, could improve upon the results of our spatiotemporal analysis. Such a study would allow us to more strongly relate the ASOS network fog measurements with the fog occurrence of the surrounding area and to understand gradients in fog occurrence from the coast inland. Additionally, more spatial information about fog patterns with co-located weather metrics will lead to an understanding of the physical drivers of spatiotemporal heterogeneity, which is critical to understand the local effects of climate change.

CRediT authorship contribution statement

Sonya Rauschenbach: Writing – review & editing, Writing – original draft, Visualization, Validation, Methodology, Investigation, Formal analysis, Data curation, Conceptualization. **John B. Kim:** Writing – review & editing, Writing – original draft, Validation, Supervision, Resources, Methodology, Funding acquisition, Formal analysis, Data curation, Conceptualization. **Alex W. Dye:** Writing – original draft, Methodology, Investigation, Data curation, Conceptualization. **Ian Faloona:** Visualization, Formal analysis. **R. Cotton Rockwood:** Conceptualization. **Christopher J. Still:** Methodology, Formal analysis, Conceptualization. **Kyaw Tha Paw U:** Writing – original draft, Supervision, Methodology, Formal analysis. **Adele L. Igel:** Writing – review & editing, Writing – original draft, Visualization, Supervision, Methodology, Formal analysis.

Declaration of competing interest

The authors declare the following financial interests/personal relationships which may be considered as potential competing interests: Sonya Rauschenbach reports financial support was provided by Earth Science Information Partners. Sonya Rauschenbach reports financial support was provided by Oak Ridge Institute for Science and Education. Sonya Rauschenbach reports financial support was provided by USDA Forest Service Pacific Northwest Region. Ian Faloona reports financial support was provided by USDA National Institute of Food and Agriculture. If there are other authors, they declare that they have no known competing financial interests or personal relationships that could have appeared to influence the work reported in this paper.

Acknowledgments

We thank Surfline.com and Dr. Rob Holman in the College of Earth, Ocean and Atmospheric Sciences at Oregon State University for freely providing camera images. We appreciate the valuable feedback from the anonymous reviewers which strengthened our manuscript. Additionally, we thank Alexander Hort, Charles Grimm, Elijah Tshilonda, Jacob Melendrez, Paul Green and Tessa Krellner for labeling fog images. S. Rauschenbach was supported in part by a grant from Earth Science Information Partners (ESIP) and a fellowship from Oak Ridge Institute for Science and Education (ORISE), with funding from USDA Forest Service Western Wildland Environmental Threat Assessment Center (23-IA-11261999-079). Additionally, I.C. Faloona's effort was supported by the USDA National Institute of Food and Agriculture, Hatch project (CA-D-LAW-2481-H).

Appendix A. Supplementary data

Supplementary material related to this article can be found online at https://doi.org/10.1016/j.agrformet.2026.111315.

Data availability

Data will be made available on request.

References

Baguskas, S.A., King, J.Y., Fischer, D.T., D'Antonio, C.M., Still, C.J., 2016a. Impact of fog drip versus fog immersion on the physiology of Bishop pine saplings. Funct. Plant Biol. 44 (3), 339–350. http://dx.doi.org/10.1071/FP16234, Retrieved 2025-05-24, from URL https://www.publish.csiro.au/fp/FP16234.

Baguskas, S.A., Still, C.J., Fischer, D.T., D'Antonio, C.M., King, J.Y., 2016b. Coastal fog during summer drought improves the water status of sapling trees more than adult trees in a California pine forest. Oecologia 181 (1), 137–148. http://dx.doi.org/10.1007/s00442-016-3556-y, Retrieved 2023-04-14, from https://doi.org/10.1007/s00442-016-3556-y.

Bassiouni, M., Scholl, M.A., Torres-Sanchez, A.J., Murphy, S.F., 2017. A method for quantifying cloud immersion in a tropical mountain forest using time-lapse photography. Agricult. Forest. Meterol. 243, 100–112. http://dx.doi.org/10.1016/j.agrformet.2017.04.010, Retrieved 2023-01-11, from https://www.sciencedirect.com/science/article/pii/S0168192317301442.

Bendix, J., Rollenbeck, R., Göttlicher, D., Nauß, T., Fabian, P., 2008. Seasonality and diurnal pattern of very low clouds in a deeply incised valley of the eastern tropical Andes (South Ecuador) as observed by a cost-effective WebCam system. Meteorol. Appl. 15 (2), 281–291. http://dx.doi.org/10.1002/met.72, Retrieved 2024-08-28, from https://onlinelibrary.wiley.com/doi/abs/10.1002/met.72. (_eprint: https://onlinelibrary.wiley.com/doi/pdf/10.1002/met.72).

Bergot, T., Koracin, D., 2021. Observation, simulation and predictability of fog: Review and perspectives. Atmosphere 12 (2), 235. http://dx.doi.org/10.3390/atmos12020235, Retrieved 2023-08-29, from https://www.mdpi.com/2073-4433/12/2/235, (Number: 2).

Breiman, L., 2001. Random forests. Mach. Learn. 45 (1), 5–32. http://dx.doi.org/10.1023/A:1010933404324, Retrieved 2026-02-04, from https://doi.org/10.1023/A:1010933404324.

Bristol, 2017. Siting Criteria for Automated Weather Observing Systems. U.S. Department of Transportation Federal Aviation Administration, Retrieved from https://www.faa.gov/documentLibrary/media/Order/6560_20c_ord.pdf.

Burk, S.D., Thompson, W.T., 1996. The summertime low-level jet and marine boundary layer structure along the California coast. Mon. Weather Rev. 124 (4), 668–686. http://dx.doi.org/10.1175/1520-0493(1996)124<0668:TSLLJA>2.0.CO;2, Retrieved 2025-02-26, from https://journals.ametsoc.org/view/journals/mwre/124/4/1520-0493_1996_124_0668_tsllja_2_0_co_2.xml.

Carbone, M.S., Park Williams, A., Ambrose, A.R., Boot, C.M., Bradley, E.S., Dawson, T.E., et al., 2013. Cloud shading and fog drip influence the metabolism of a coastal pine ecosystem. Global Change Biol. 19 (2), 484–497. http://dx.doi.org/10.1111/gcb.12054, Retrieved 2023-04-26, from https://onlinelibrary.wiley.com/doi/abs/10.1111/gcb.12054. (_eprint: https://onlinelibrary.wiley.com/doi/pdf/10.1111/gcb.12054).

Choi, L.K., You, J., Bovik, A.C., 2015. Referenceless prediction of perceptual fog density and perceptual image defogging. IEEE Trans. Image Process. 24 (11), 3888–3901. http://dx.doi.org/10.1109/TIP.2015.2456502, Conference Name: IEEE Transactions on Image Processing.

Clemesha, R.E.S., Gershunov, A., Iacobellis, S.F., Williams, A.P., Cayan, D.R., 2016. The northward march of summer low cloudiness along the California coast. Geophys. Res. Lett. 43 (3), 1287–1295. http://dx.doi.org/10.1002/2015GL067081, Retrieved 2023-01-23, from https://onlinelibrary.wiley.com/doi/abs/10.1002/2015GL067081. (_eprint: https://onlinelibrary.wiley.com/doi/pdf/10.1002/2015GL067081).

Dorman, C.E., Mejia, J., Koračin, D., McEvoy, D., 2020. World marine fog analysis based on 58-years of ship observations. Int. J. Climatol. 40 (1), 145–168. http://dx.doi.org/10.1002/joc.6200, Retrieved 2024-09-29, from https://onlinelibrary.wiley.com/doi/abs/10.1002/joc.6200. (_eprint: https://onlinelibrary.wiley.com/doi/pdf/10.1002/joc.6200).

Dye, A., Rastogi, B., Clemesha, R.E.S., Kim, J.B., Samelson, R.M., Still, C.J., Williams, A.P., 2020. Spatial patterns and trends of summertime low cloudiness for the Pacific Northwest, 1996–2017. Geophys. Res. Lett. 47 (16), e2020GL088121. http://dx.doi.org/10.1029/2020GL088121, Retrieved 2023-01-11, from https://onlinelibrary.wiley.com/doi/abs/10.1029/2020GL088121. (_eprint: https://onlinelibrary.wiley.com/doi/pdf/10.1029/2020GL088121).

Dye, A., Rauschenbach, S., de Szoeke, S., Igel, A.L., Jin, Y., Kim, J.B., et al., 2024. Fog in western coastal ecosystems: inter-disciplinary challenges and opportunities with example concepts from the Pacific Northwest, USA. Front. Environ. Sci. 12, http://dx.doi.org/10.3389/fenvs.2024.1488401, Retrieved 2024-11-29, from https://www.frontiersin.org/journals/environmental-science/articles/10.3389/fenvs.2024.1488401/full.

Earth Resources Observation and Science (EROS) Center, 2025. Annual NLCD (National Land Cover Database)—The next generation of land cover mapping. SGS Publications Warehouse, http://dx.doi.org/10.3133/fs20253001.

Environment Canada, 2017. Manual of Marine Weather Observations. Meteorological Service of Canada, Retrieved from https://www.canada.ca/en/environment-climate-change/services/weather-manuals-documentation/marine-observations.html.

Farr, T.G., Rosen, P.A., Caro, E., Crippen, R., Duren, R., Hensley, S., et al., 2007. The shuttle radar topography mission. Rev. Geophys. 45 (2), http://dx.doi.org/10.1029/2005RG000183, Retrieved 2025-06-11, from https://onlinelibrary.wiley.com/doi/abs/10.1029/2005RG000183. (_eprint: https://onlinelibrary.wiley.com/doi/pdf/10.1029/2005RG000183).

Filonczuk, M.K., Cayan, D.R., Riddle, L.G., 1995. Variability of marine fog along the California coast. Retrieved 2025-02-27, from https://escholarship.org/uc/item/2kc7x97f.

Fischer, D.T., Still, C.J., Williams, A.P., 2009. Significance of summer fog and overcast for drought stress and ecological functioning of coastal California endemic plant species. J. Biogeogr. 36 (4), 783–799. http://dx.doi.org/10.1111/j.1365-2699.2008.02025.x, Retrieved 2023-07-08, from https://onlinelibrary.wiley.com/doi/abs/10.1111/j.1365-2699.2008.02025.x. (_eprint: https://onlinelibrary.wiley.com/doi/pdf/10.1111/j.1365-2699.2008.02025.x).

Iacobellis, S.F., Cayan, D.R., 2013. The variability of California summertime marine stratus: Impacts on surface air temperatures. J. Geophys. Res.: Atmos. 118 (16), 9105–9122. http://dx.doi.org/10.1002/jgrd.50652, Retrieved 2025-02-26, from https://onlinelibrary.wiley.com/doi/abs/10.1002/jgrd.50652. (_eprint: https://onlinelibrary.wiley.com/doi/pdf/10.1002/jgrd.50652).

Isaac, G.A., Bullock, T., Beale, J., Beale, S., 2020. Characterizing and predicting marine fog offshore newfoundland and labrador. Weather. Forecast. 35 (2), 347–365. http://dx.doi.org/10.1175/WAF-D-19-0085.1, Retrieved 2026-04-25, from https://journals.ametsoc.org/view/journals/wefo/35/2/waf-d-19-0085.1.xml.

Izett, J.G., van de Wiel, B.J.H., Baas, P., van Hooft, J.A., Schulte, R.B., 2019. Dutch fog: On the observed spatio-temporal variability of fog in the Netherlands. Q. J. R. Meteorol. Soc. 145 (723), 2817–2834. http://dx.doi.org/10.1002/qj.3597, Retrieved 2024-07-05, from https://onlinelibrary.wiley.com/doi/abs/10.1002/qj.3597. (_eprint: https://onlinelibrary.wiley.com/doi/pdf/10.1002/qj.3597).

Johnstone, J.A., Dawson, T.E., 2010. Climatic context and ecological implications of summer fog decline in the coast redwood region. Proc. Natl. Acad. Sci. 107 (10), 4533–4538. http://dx.doi.org/10.1073/pnas.0915062107, Retrieved 2023-01-12, from https://www.pnas.org/doi/10.1073/pnas.0915062107.

Kim, K.W., 2018. The comparison of visibility measurement between image-based visual range, human eye-based visual range, and meteorological optical range. Atmos. Environ. 190, 74–86. http://dx.doi.org/10.1016/j.atmosenv.2018.07.020, Retrieved 2026-02-09, from https://www.sciencedirect.com/science/article/pii/S1352231018304679.

Li, H.-J., Lo, M.-H., Juang, J.-Y., Wang, J., Huang, C.-y., 2022. Assessment of spatiotemporal dynamics of diurnal fog occurrence in subtropical montane cloud forests. Agricult. Forest. Meterol. 317, 108899. http://dx.doi.org/10.1016/j.agrformet.2022.108899, Retrieved 2024-08-28, from https://www.sciencedirect.com/science/article/pii/S0168192322000922.

Limm, E.B., Simonin, K.A., Bothman, A.G., Dawson, T.E., 2009. Foliar water uptake: a common water acquisition strategy for plants of the redwood forest. Oecologia 161 (3), 449–459. http://dx.doi.org/10.1007/s00442-009-1400-3, Retrieved 2023-02-24, from https://doi.org/10.1007/s00442-009-1400-3.

Lundberg, S., Lee, S.-I., 2017. A unified approach to interpreting model predictions. http://dx.doi.org/10.48550/arXiv.1705.07874, arXiv. Retrieved 2024-06-23, from http://arxiv.org/abs/1705.07874 (arXiv:1705.07874 [cs, stat]).

Lundquist, J.D., Bourcy, T.B., 2000. California and Oregon Humidity and Coastal Fog. Scripps Institution of Oceanography, La Jolla, California.

Nuss, W.A., Bane, J.M., Thompson, W.T., Holt, T., Dorman, C.E., Ralph, F.M., et al., 2000. Coastally trapped wind reversals: Progress toward understanding. Bull. Am. Meteorol. Soc. 81 (4), 719–744. http://dx.doi.org/10.1175/1520-0477(2000)081<0719:CTWRPT>2.3.CO;2, Retrieved 2025-05-26, from https://journals.ametsoc.org/view/journals/bams/81/4/1520-0477_2000_081_0719_ctwrpt_2_3_co_2.xml.

O'Brien, T.A., Sloan, L.C., Chuang, P.Y., Faloona, I.C., Johnstone, J.A., 2013. Multidecadal simulation of coastal fog with a regional climate model. Clim. Dyn. 40 (11), 2801–2812. http://dx.doi.org/10.1007/s00382-012-1486-x, Retrieved 2023-02-10, from https://doi.org/10.1007/s00382-012-1486-x.

Pagani, G.A., Noteboom, J.W., Wauben, W., Observations, D., Box, P.O., Bilt, A.D., 2018. Deep Neural Network Approach for Automatic Fog Detectopm using Traffic Camera Images. Royal Netherlands Meteorological Institute (KNMI).

Pedregosa, F., Varoquaux, G., Gramfort, A., Michel, V., Thirion, B., Grisel, O., et al., 2011. Scikit-learn: Machine learning in python. J. Mach. Learn. Res. 12, 2825–2830.

Petty, G.W., 2008. A First Course in Atmospheric Thermodynamics. Sundog Publishing.

Ramlakhan, Z., 2015. https://cdn.knmi.nl/knmi/pdf/bibliotheek/knmipubIR/IR2015-05.pdf Retrieved 2024-08-28, from https://cdn.knmi.nl/knmi/pdf/bibliotheek/knmipubIR/IR2015-05.pdf.

Rasmussen, C.E., Williams, C.K.I., 2006. Gaussian Processes for Machine Learning. MIT Press, Cambridge, Mass, (OCLC: ocm61285753).

Rastogi, B., Williams, A.P., Fischer, D.T., Iacobellis, S.F., McEachern, K., Carvalho, L., et al., 2016. Spatial and temporal patterns of cloud cover and fog inundation in coastal California: Ecological implications. Earth Interactions 20 (15), 1–19. http://dx.doi.org/10.1175/EI-D-15-0033.1, Retrieved 2023-04-14, from https://journals.ametsoc.org/view/journals/eint/20/15/ei-d-15-0033.1.xml.

Rijsbergen, C.J.V., 1979. Information Retrieval. Butterworths.

del Río, C., Lobos, F., Siegmund, A., Tejos, C., Osses, P., Huaman, Z., et al., 2021. GOFOS, ground optical fog observation system for monitoring the vertical stratocumulus-fog cloud distribution in the coast of the Atacama Desert, Chile. J. Hydrol. 597, 126190. http://dx.doi.org/10.1016/j.jhydrol.2021.126190, Retrieved 2024-07-24, from https://www.sciencedirect.com/science/article/pii/S0022169421002377.

Schulz, H.M., Chang, S.-C., Thies, B., Bendix, J., 2014. Automatic cloud top height determination in mountainous areas using a cost-effective time-lapse camera system. Atmos. Meas. Tech. 7 (12), 4185–4201. http://dx.doi.org/10.5194/amt-7-4185-2014, Retrieved 2024-08-28, from https://amt.copernicus.org/articles/7/4185/2014/.

Schwartz, R.E., Gershunov, A., Iacobellis, S.F., Cayan, D.R., 2014. North American west coast summer low cloudiness: Broadscale variability associated with sea surface temperature. Geophys. Res. Lett. 41 (9), 3307–3314. http://dx.doi.org/10.1002/2014GL059825, Retrieved 2024-08-20, from https://onlinelibrary.wiley.com/doi/abs/10.1002/2014GL059825. (_eprint: https://onlinelibrary.wiley.com/doi/pdf/10.1002/2014GL059825).

Tardif, R., Rasmussen, R.M., 2007. Event-based climatology and typology of fog in the New York city region. J. Appl. Meteorol. Clim. 46 (8), 1141–1168. http://dx.doi.org/10.1175/JAM2516.1, Retrieved 2024-07-06, from https://journals.ametsoc.org/view/journals/apme/46/8/jam2516.1.xml.

Torregrosa, A., Combs, C., Peters, J., 2016. GOES-derived fog and low cloud indices for coastal north and central California ecological analyses. Earth Space Sci. 3 (2), 46–67. http://dx.doi.org/10.1002/2015EA000119, Retrieved 2023-02-10, from https://onlinelibrary.wiley.com/doi/abs/10.1002/2015EA000119. (_eprint: https://onlinelibrary.wiley.com/doi/pdf/10.1002/2015EA000119).

Torregrosa, A., O'Brien, T.A., Faloona, I.C., 2014. Coastal fog, climate change, and the environment. Eos, Trans. Am. Geophys. Union 95 (50), 473–474. http://dx.doi.org/10.1002/2014EO500001, Retrieved 2023-02-10, from http://doi.wiley.com/10.1002/2014EO500001.

Walt, S.v.d., Schönberger, J.L., Nunez-Iglesias, J., Boulogne, F., Warner, J.D., Yager, N., et al., 2014. Scikit-image: image processing in python. PeerJ 2, e453. http://dx.doi.org/10.7717/peerj.453, Retrieved 2025-05-25, from https://peerj.com/articles/453.

Wauben, W., Roth, M., 2016. https://www.wmocimo.net/eventpapers/session2/O2(8)_Wauben_Camera-fog-visibility.pdf. Retrieved 2024-08-28, from https://www.wmocimo.net/eventpapers/session2/O2(8)_Wauben_Camera-fog-visibility.pdf.

Williams, A.P., Schwartz, R.E., Iacobellis, S., Seager, R., Cook, B.I., Still, C.J., et al., 2015. Urbanization causes increased cloud base height and decreased fog in coastal Southern California. Geophys. Res. Lett. 42 (5), 1527–1536. http://dx.doi.org/10.1002/2015GL063266, Retrieved 2023-08-24, from https://onlinelibrary.wiley.com/doi/abs/10.1002/2015GL063266. (_eprint: https://onlinelibrary.wiley.com/doi/pdf/10.1002/2015GL063266).

Williams, A.P., Still, C.J., Fischer, D.T., Leavitt, S.W., 2008. The influence of summertime fog and overcast clouds on the growth of a coastal Californian pine: a tree-ring study. Oecologia 156 (3), 601–611. http://dx.doi.org/10.1007/s00442-008-1025-y, Retrieved 2023-07-08, from https://doi.org/10.1007/s00442-008-1025-y.

WMO, 2024. International Cloud Atlas, World Meteorology Organization. World Meteorology Organization, Retrieved 2025-02-26, from https://cloudatlas.wmo.int/home.html.

Xu, Q.-S., Liang, Y.-Z., 2001. Monte Carlo cross validation. Chemometr. Intell. Lab. Syst. 56 (1), 1–11. http://dx.doi.org/10.1016/S0169-7439(00)00122-2, Retrieved 2024-08-16, from https://www.sciencedirect.com/science/article/pii/S0169743900001222.

Zhang, D., Sullivan, T., O'Connor, N.E., Gillespie, R., Regan, F., 2015. Coastal fog detection using visual sensing. In: OCEANS 2015 - Genova. pp. 1–5. http://dx.doi.org/10.1109/OCEANS-Genova.2015.7271683, Retrieved 2024-07-16, from https://ieeexplore.ieee.org/abstract/document/7271683.